SN Applied Sciences

Electrospun polyester-urethane scaffold preserves mechanical properties and exhibits strain stiffening during in situ tissue ingrowth and degradation

--Manuscript Draft--

Manuscript Number:	SNAS-D-19-07383R1
Full Title:	Electrospun polyester-urethane scaffold preserves mechanical properties and exhibits strain stiffening during in situ tissue ingrowth and degradation
Article Type:	Research Article
Section/Category:	Engineering: TC: Applied Mechanics and Materials Engineering (AMME)
Funding Information:	South African Medical Research Council (N/A) — Prof Thomas Franz National Research Foundation (N/A) — Prof Thomas Franz International Society of Biomechanics (N/A) — Dr Hugo Krynauw Deutsche Herzstiftung (S/08/10) — Dr Josepha Koehne
Abstract:	Consistent mechanical performance from implantation through healing and scaffold degradation is highly desired for tissue-regenerative scaffolds, e.g. when used for vascular grafts. The aim of this study was the paired in vivo mechanical assessment of biostable and fast degrading electrospun polyester-urethane scaffolds to isolate the effects of material degradation and tissue formation after implantation. Biostable and degradable polyester-urethane scaffolds with substantial fibre alignment were manufactured by electrospinning. Scaffold samples were implanted paired in subcutaneous position in rats for 7, 14 and 28 days. Morphology, mechanical properties and tissue ingrowth of the scaffolds were assessed before implantation and after retrieval. Tissue ingrowth after 28 days was 83 ± 10% in the biostable scaffold and 77 ± 4% in the degradable scaffold. For the biostable scaffold, the elastic modulus at 12% strain increased significantly between 7 and 14 days and decreased significantly thereafter in fibre but not in cross-fibre direction. The degradable scaffold exhibited a significant increase in the elastic modulus at 12% strain from 7 to 14 days after which it did not decrease but remained at the same magnitude, both in fibre and in cross-fibre direction. Considering that the degradable scaffold loses its material strength predominantly during the first 14 days of hydrolytic degradation (as observed in our previous in vitro study), the consistency of the elastic modulus of the degradable scaffold after 14 days is an indication that the regenerated tissue construct retains it mechanical properties.
Keywords:	Electrospinning; elastic modulus; mechanical properties; soft tissue regeneration; degradation
Corresponding Author:	Thomas Franz University of Cape Town SOUTH AFRICA
Corresponding Author Secondary Information:	
Corresponding Author's Institution:	University of Cape Town
Corresponding Author's Secondary Institution:	
First Author:	Hugo Krynauw
First Author Secondary Information:	
Order of Authors:	Hugo Krynauw Rodaina Omar Josepha Koehne

	Georges Limbert
	Neil Davies
	Deon Bezuidenhout
	Thomas Franz
Order of Authors Secondary Information:	
Author Comments:	3 March 2020 RE: Submission of Revised Manuscript Please find enclosed our revised manuscript entitled “Electrospun polyester-urethane scaffold preserves mechanical properties and exhibits strain stiffening during in situ tissue ingrowth and degradation” co-authored by Hugo Krynauw, Rodaina Omar, Josepha Koehne, Georges Limbert, Neil H Davies, Deon Bezuidenhout, and Thomas Franz. Please address all correspondence to: Thomas Franz Department of Human Biology Faculty of Health Sciences University of Cape Town Private Bag X3 Observatory 7935 South Africa Tel.: +27 21 650 1795 Email: thomas.franz@uct.ac.za Sincerely, Thomas Franz
Response to Reviewers:	Response to Reviewers Reviewer #1: COMMENT 1. More literature review to be added. RESPONSE: We have expanded the literature review. COMMENT 2. Formatting not proper. RESPONSE: We have improved formatting COMMENT 3. More technical analysis to be added. RESPONSE: It is not clear which additional technical analysis the reviewer proposes and we unfortunately could not address this comment. COMMENT 4. If possible add mathematical equations. RESPONSE: It is not clear where the reviewer see more mathematical equations, as such we unfortunately could not address this comment. Reviewer #2: The manuscript describes the change in mechanical stiffnes of polymer scaffolds during tissue ingrowth and compares a degradable and non-degradable vaiant of the same material. It is found that the degradable scaffold gains in mechnical strengh upon tissue ingrowth, indicating that the effect of such is more than enough to compensate for the degradation. The manuscript is well written and can be published after some minor errors in the methods section are adressed: COMMENT P4. l7. "hydroxybutirrate" should probably be "hydroxybutyrate". RESPONSE: We have corrected this.

	COMMENT P4 l33. "electrostatic field" should, judging from the unit, be "potential difference" (the field would then be [potential difference]/[source-target distance]) RESPONSE: We have corrected this. COMMENT Eq 3. The plus sign in second paranthesis of the denominator in the middle expression should be a minus sign. RESPONSE: We have corrected this. Reviewer #3: COMMENT May be accepted
Suggested Reviewers:	

Original Research

Electrospun polyester-urethane scaffold preserves mechanical properties and exhibits strain stiffening during *in situ* tissue ingrowth and degradation

Hugo Krynauw[1,2], Rodaina Omar[2], Josepha Koehne[2], Georges Limbert[1,3], Neil H Davies[2], Deon Bezuidenhout[2], Thomas Franz[1,3,*]

[1]Division of Biomedical Engineering, Department of Human Biology, University of Cape Town, Observatory, South Africa

[2]Cardiovascular Research Unit, Chris Barnard Division of Cardiothoracic Surgery, University of Cape Town, Observatory, South Africa

[3]National Centre for Advanced Tribology & Bioengineering Science Research Group, Department of Mechanical Engineering Sciences, Faculty of Engineering and Physical Sciences, University of Southampton, Southampton, UK

* Corresponding author: Email: thomas.franz@uct.ac.za

ORCID IDs:
HK: 0000-0001-9713-8396
RO:
JK: 0000-0003-3140-4887
GL: 0000-0002-4268-6106
NHD: 0000-0003-0432-4515
DB: 0000-0001-8052-7491
TF: 0000-0002-1504-3842

DECLARATIONS
Funding: This study was supported financially by the National Research Foundation of South Africa and the South African Medical Research Council. HK received a matching dissertation grant from the International Society of Biomechanics. JK acknowledges financial support from the Deutsche Herzstiftung (Jahresstipendium S/08/10).
Conflicts of interest: The authors declare that they do not have conflicts of interests.
Ethics approval: All animal experiments were authorised by the Faculty of Health Sciences Research Ethics Committee of the University of Cape Town and were performed in accordance with the National Institutes of Health (NIH, Bethesda, MD) guidelines.
Consent to participate: Not applicable
Consent for publication: Not applicable
Availability of data and material: Quantitative data for fibre diameter, fibre alignment, tissue ingrowth and mechanical characterisation are available on ZivaHUB (http://doi.org/10.25375/uct.9892367).
Code availability: Not applicable
Acknowledgements: The authors thank ab medica S.p.A for donating the DegraPol® material for this study. ETH Zurich and the University of Zurich are owners and ab medica S.p.A is exclusive licensee of all Intellectual Property Rights of DegraPol®.

Abstract

Consistent mechanical performance from implantation through healing and scaffold degradation is highly desired for tissue-regenerative scaffolds, e.g. when used for vascular grafts. The aim of this study was the paired *in vivo* mechanical assessment of biostable and fast degrading electrospun polyester-urethane scaffolds to isolate the effects of material degradation and tissue formation after implantation. Biostable and degradable polyester-urethane scaffolds with substantial fibre alignment were manufactured by electrospinning. Scaffold samples were implanted paired in subcutaneous position in rats for 7, 14 and 28 days. Morphology, mechanical properties and tissue ingrowth of the scaffolds were assessed before implantation and after retrieval. Tissue ingrowth after 28 days was 83 ± 10% in the biostable scaffold and 77 ± 4% in the degradable scaffold. For the biostable scaffold, the elastic modulus at 12% strain increased significantly between 7 and 14 days and decreased significantly thereafter in fibre but not in cross-fibre direction. The degradable scaffold exhibited a significant increase in the elastic modulus at 12% strain from 7 to 14 days after which it did not decrease but remained at the same magnitude, both in fibre and in cross-fibre direction. Considering that the degradable scaffold loses its material strength predominantly during the first 14 days of hydrolytic degradation (as observed in our previous *in vitro* study), the consistency of the elastic modulus of the degradable scaffold after 14 days is an indication that the regenerated tissue construct retains it mechanical properties.

Keywords: Electrospinning; elastic modulus; mechanical properties; soft tissue regeneration; degradation

Article Highlights:

- Stiffness of fast-degrading fibrous DegraPol® scaffold is maintained during tissue ingrowth
- Stiffness of scaffold with ingrown tissue increases with increasing deformation – resembling biological tissue such as arteries

1. Introduction

Regenerative medicine has emerged as one of the most dynamic drivers in the development of advanced engineered biomaterial solutions for tissue engineering applications [1,2]. One crucial element in regenerative medicine are scaffolds that facilitate and guide the regeneration of biological tissues according to the biophysical requirements of the specific application.

The ideal conduit for arterial replacement or bypass remains autologous grafts, i.e. the patient's own artery or vein. Autologous grafts are, however, often unavailable due to either disease or previous use for bypass grafting [3-7]. Whereas currently available vascular prostheses made from polyethylene terephthalate (PET) such as Dacron®, and expanded polytetrafluoroethylene (ePTFE) perform well as large-calibre replacements, their long-term patency is discouraging in small to medium graft (<7 mm) applications [3,4,8]. This limitation is mainly a result of a poor healing process with surface thrombogenicity due to the lack of endothelial cells, as well as anastomotic intimal hyperplasia [5,9]. Although attempts have been made to improve these grafts by means of various coatings, the results are not conclusive [5,10-12].

Tissue engineering and regeneration has provided a promising avenue for the development of vascular grafts. The ideal scaffold facilitates tissue regeneration such that the new tissue constructs mimics biologically and mechanically the healthy vascular tissue [2]. For small-to-medium diameter tissue engineered or tissue regenerative vascular grafts, a key factor for long term success is porosity [8]. The complete healing of the porous vascular graft implies interconnected pores to permit transmural tissue ingrowth [8,13,14].

Several approaches have been used to obtain porous polymeric scaffolds for vascular grafts, including particulate leaching [14-16], thermally induced phase separation [17,18]. Another method of introducing porosity in vascular scaffolds is electrospinning [19-24]. Here, the adjustment of process parameters allows controlling the degree of fibre alignment in the resulting polymeric network [25,26]. Fibre alignment strongly determines the mechanical properties of the scaffold [9]. Random fibre alignment leads to mechanical isotropy of the scaffold, which exhibits similar properties in different directions. In contrast, the predominant alignment of fibres in one direction introduces mechanical anisotropy [26].

Electro-spun scaffolds with a high degree of fibre alignment exhibit the highest elastic modulus, i.e. stiffness, in direction of the predominant fibre alignment and the lowest elastic modulus perpendicular to the fibre alignment. Mechanical anisotropy can offer a useful tool to tailor the structural properties of the scaffold but also adds complexity to the design process. The latter needs to be addressed

adequately, in particular for biodegradable scaffolds and considering that tissue regenerating in the scaffold will contribute to structural and mechanical properties of the regenerating tissue construct.

Scaffold degradation and tissue incorporation are transient processes, and gradual change of the mechanical properties of the scaffold-tissue construct is expected until degradation and tissue ingrowth are complete. Biomechanical properties of scaffolds were predominantly obtained prior to tissue culturing or implantation [19,22,27-30] whereas the changes in mechanical properties due to *in situ* tissue ingrowth after implantation in fast-degrading scaffolds have received very little attention.

In previous studies, we separately quantified the effect of *in vitro* degradation [31] and *in situ* tissue ingrowth in a biostable scaffold [32] on the scaffolds' mechanical properties. The present study aimed at investigating the combined effects of concurrent *in situ* tissue ingrowth and scaffold degradation on the mechanical properties of a fast-degrading electrospun polyester-urethane scaffold. Matched implants of the polyester-urethane scaffold with a fast-degrading and a non-degrading formulation, respectively, served as internal controls.

2. Materials and Methods

2.1 Material

DegraPol® (ab medica S.p.A, Cerro Maggiore, MI, Italy), a biodegradable polyester-urethane that consists of poly(ε-caprolactone-co-glycolide)-diol soft segments and poly(3-(R-hydroxybutyrate)-co-(ε-caprolactone))-diol hard segments was used. Both polymer segments are biodegradable and their degradation products are non-toxic [33]. The mechanical properties of the polymer can be modulated by adjusting the ratio of the hard and soft segments. Changing the ratio of ε-caprolactone to glycolide affects the degradation characteristics. DegraPol® DP0 and DP30 have ε-caprolactone-to-glycolide ratio of 100:0 and 70:30 respectively, and both have a hard-to-soft segment ratio of 40:60 (unpublished data).

2.2 Electro-spinning and sample preparation

DegraPol® DP0 and DP30 were each dissolved in chloroform at room temperature with subsequent sonication in distilled water at 37°C for 90 min to obtain polymer solutions of 24% by weight concentration. The DegraPol® solution was electro-spun from a hypodermic needle (SE400B syringe pump, Fresenius, Bad Homburg, Germany) onto a rotating and bi-directionally translating tubular target (hypodermic tubing, Small Parts, Loganport, IN, USA) using a custom-made rig. The spinning parameters were: solution flow rate of 4.8 mL/h, target outer diameter of 25 mm, target rotating speed of 9600 rpm, target translational speed of 2.6 mm/min, potential difference of 15 kV, and source-target distance of 250 mm. After completion of the spinning process, the electro-spun structure on the

target hypotube was submersed in ethanol for 5 minutes, removed from the mandrel and dried under vacuum (Townson & Mercer Ltd, Stretford, England; room temperature, 90 min) and trimmed on either end to discard regions with decreasing wall thickness. Tubular scaffolds were cut into rectangular samples with the longer edge aligned with either the circumferential (C) or axial (A) direction of the tube. Samples underwent standard ethylene oxide sterilisation (55°C, 60% relative humidity, 12 h) and were subsequently placed in vacuum for 6 h to allow removal of ethylene oxide.

2.3 Physical characterisation of scaffold before implantation

Physical characterisation included microscopic analysis of fibre diameter and alignment, measurement of scaffold wall thickness and porosity as described previously [32].

2.3.1 Fibre diameter and alignment

Scanning electron microscope (SEM) images were obtained (Nova NanoSEM 230, FEI, Hillsboro, OR, US) of samples after sputter-coating with gold (Polaron SC7640, Quorum Technologies, East Grinstead, UK). The fibre diameter was measured on x750 SEM micrographs with Scion Image (Scion Corporation, Frederick, USA) (n = 3 samples; 4 images per sample, i.e. one image from two different locations of each sample surface; ten measurements per image). Fibre alignment was quantified on x100 SEM images using Fiji [34], by means of Fourier component analysis with the Directionality plug-in (written by JeanYves Tinevez) as described by Woolley et al. [35]. The analysis provides a dispersion factor as a measure of alignment of the fibres with smaller dispersion values indicating higher degree of alignment.

2.3.2 Sample dimensions

Width, length and thickness of scaffold samples were measured on macroscopic images obtained with a Leica DFC280 stereo microscope using Leica IM500 imaging software (Leica Microsystems GmbH, Wetzlar, Germany).

2.3.3 Scaffold porosity

Scaffold porosity, P, was determined by hydrostatic weighing typically employed for density determination. The porosity of fibrous networks is described as volumetric ratio

$$P = \frac{V_{pores}}{V_{total}} = \frac{V_{pores}}{V_{pores} + V_{fibres}}, \tag{1}$$

and when expressing volumes as masses in the form of

$$P = \frac{m_{eth.pores}}{m_{eth.pores} + m_{eth.fibres}}. \tag{2}$$

Introducing measurable quantities m_{wet}, m_{dry} and $m_{submerged}$ provides

$$P = \frac{m_{wet}-m_{dry}}{m_{wet}-m_{submerged}} = \frac{(m_{fibres}+m_{et\square.pores})-(m_{fibres})}{(m_{fibres}+m_{et\square.pores})-(m_{fibres}-m_{et\square.fibres})} = \frac{m_{et\square.pores}}{m_{et\square.pores}+m_{et\square.fibres}}, \quad (3)$$

with m_{dry} as the mass of the dry scaffold, $m_{submerged}$ as the mass of the scaffold submerged in ethanol, and m_{wet} as the scaffold mass after removal from the ethanol while ethanol is retained in the pores. The porosity was measured with n = 1 per spun scaffold.

2.4 Molecular weight

Weight-average molar weight, M_W, during degradation was determined by gel permeation chromatography (GPC) using tuneable absorbance detector (Waters 486, set to 260 nm), high-performance liquid chromatography pump (Waters 510), differential refractometer (Waters 410) and auto sampler (Spectra Series AS100, Thermo Separations). Five columns (Styragels HR1 through HR6, Waters) and a pre-column filter were used at 30°C. Polystyrene standards were used for calibration. Samples were dissolved in tetrahydrofuran (1 mg/ml, 37°C, sonication for 20 min). A sample volume of 180 µl was injected with a flow rate of 1.06 ml/min.

2.5 Study design

This study used a subcutaneous rat model with implant durations of 7, 14 and 28 days and n = 10 animals per each time point. Each animal received six implants, namely thee biostable DP0 scaffold samples and three biodegradable DP30 scaffold samples.

2.6 Implantation procedure

All animal experiments were authorised by the Faculty of Health Sciences Research Ethics Committee of the University of Cape Town and were performed in accordance with the National Institutes of Health (NIH, Bethesda, MD) guidelines.

Male Wistar albino rats with body mass 200-250 g were used. Anaesthesia was induced by placing the animal in an inhalation chamber with an air flow of 5% isoflurane for 5 min. The animals were shaved and sterilized with iodine in the area of the incision. Anaesthesia was maintained by nose cone delivery of 1.5% isoflurane at an oxygen output of 1.5 L/min at 1 bar and 21°C. The body temperature of the animals was maintained throughout the surgical procedure by placing the animal on a custom-made heating pad at 37°C.

Six longitudinal incisions of 1 cm (three on either side of the dorsal midline) were made and subcutaneous pockets of 2 cm depth bluntly dissected. Scaffold samples were placed within the

pockets and incisions closed with silk 4/0 (Ethicon Inc, Somerville, NJ) interrupted sutures in a subcuticular fashion.

2.7 Implant retrieval

Anaesthesia was induced by placing the animal in an inhalation chamber with an air flow of 5% isoflurane for 5 min. Rats were euthanized by inhalation of 5% halothane in air followed by a cardiac injection of 1 ml saturated KCl solution. The samples with surrounding tissue were excised. Samples for mechanical testing were submerged in phosphate buffered saline (PBS) solution and stored at 4°C. Samples for histological analysis underwent tissue fixation in 10% formalin (Sigma Aldrich, Steinheim, Germany) for 48 hours and transferred into 70% ethanol solution for storage.

2.8 Mechanical testing

Prior to testing, the thickness, length and width of retrieved samples were determined with a calliper. Tensile testing was performed within 12 hours of implant retrieval with samples submerged in PBS at 37°C (Instron 5544, 10 N load cell; Instron, Norwood, USA). Samples were fixed using custom-made clamps resulting in a gauge length of approximately 10 mm. The direction of tensile load represented either circumferential (C samples) or axial direction (A samples) of the original tubular scaffold.

Pre-implant samples (T = 0 days) underwent a loading protocol comprising either (1) one initial extension to 12% strain, five cycles between 12% and 8% strain, and a final extension to failure or maximum force of 7.4 N (all at strain rate of 9.6 %/min); or (2) one single extension to 16% strain at 9.6 %/min. Retrieved implant samples were not subjected to loading cycling but underwent one single extension only (to 16% strain at 9.6 %/min) to avoid inducing structural damage in the degraded samples at the latter stages of the study. Stress-strain data obtained for pre-implant scaffold samples with and without load-cycling was used to derive a scaling function $S_C(\varepsilon) = \sigma_{Cycled}(\varepsilon)/\sigma_{Noncycled}(\varepsilon)$ that quantifies the mechanical effect of the load-cycling. Stress-strain data obtained without load cycling on retrieved scaffold samples were adjusted using S_C for each test and average data calculated. Characteristic mechanical measures were derived from these data, namely stress $\sigma_{12\%}$ at 12% strain and $\sigma_{16\%}$ at 16% strain, and elastic modulus $E_{6\%}$ at 6% strain and $E_{12\%}$ at 12% strain. (Note: Stress and strain always refers to nominal stress and Cauchy strain, respectively.)

2.9 Histology, light microscopy and assessment of tissue ingrowth

Fixed samples underwent tissue processing and paraffin embedding. Sections of 3 μm thickness were prepared from mid sample regions and stained with haematoxylin and eosin (H&E) for nuclei and cytoplasm. Microscopic images were acquired with a Nikon Eclipse 90i microscope with digital camera DXM-1200C (Nikon Corporation, Tokyo, Japan).

Tissue ingrowth was quantified by morphometric image analysis classifying areas as open space or tissue (VIS Visiopharm Integrator System, Visiopharm, Hørsholm, Denmark). A region of interest (ROI) in the image was segmented in tissue (nuclei, cytoplasm and extracellular matrix) and open space with an untrained k-means clustering technique. The algorithm classified scaffold fibres as open space since the polymer did not stain. This was corrected by adjusting for scaffold porosity.

2.10 Statistical analysis

For quantitative data, one-way ANOVA was performed when more than two groups were compared, using Tukey HSD post-hoc analysis with $p < 0.05$ indicating statistical significance. Data are provided as mean values ± standard deviation.

3. Results

SEM micrographs of the electrospun DegraPol® DP0 and DP30 scaffolds are shown in **Figure 1**. Fibre diameter (13.0 ± 2.2 µm vs 12.7 ± 4.1 µm) and scaffold porosity (74.0 ± 3.2% vs 77.0 ± 2.7%) agreed reasonably well between DP0 and DP30. The fibre dispersion was lower (i.e. fibre alignment was higher) in DP0 scaffolds (9.6 ± 2.0°) compared to DP30 scaffolds (17.8 ± 4.6°, $p < 0.05$). Scaffolds of both materials exhibited some degree of fibre merging (**Figure 1** bottom row). Morphological scaffold data and dimensions of the scaffold samples for implantation are summarised in **Table 1**.

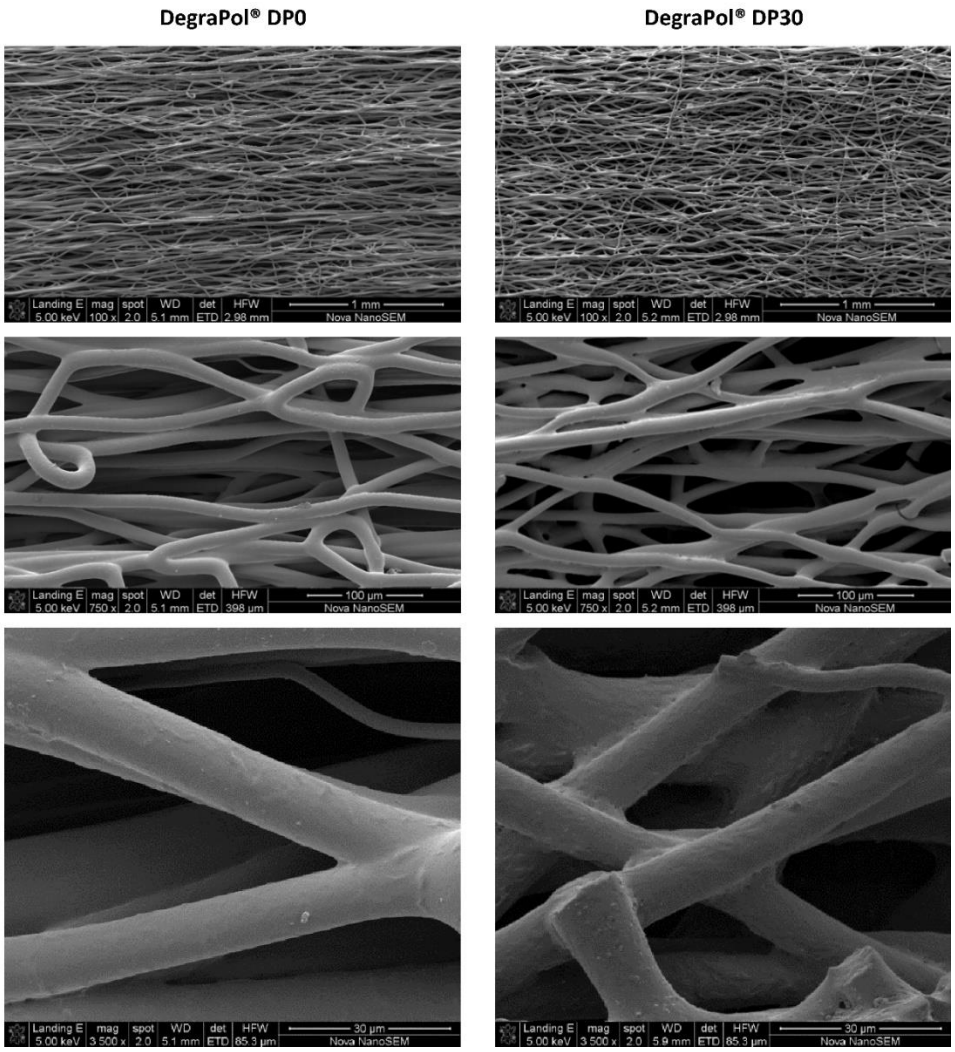

Figure 1. SEM micrographs of electrospun DegraPol® DP0 and DP30 scaffold at magnification of 100x (top), 750x (middle) and 3500x (bottom).

Table 1. Morphometric properties of the electrospun scaffolds

Parameter	**n**	**DegraPol® DP0**	**n**	**DegraPol® DP30**
Porosity	7	74.0 ± 3.2%	6	77.0 ± 2.7%
Fibre diameter	3	13.0 ± 2.2 µm	3	12.7 ± 4.1 µm
Dispersion (Goodness)	6	9.6 ± 2.0° (0.97 ± 0.01)	6	17.8 ± 4.6° (0.98 ± 0.01)
Width	70	8.6 ± 0.5 mm	68	8.1 ± 0.5 mm
Thickness	70	1.2 ± 0.2 mm	68	1.2 ± 0.2 mm
Length	70	11.1 ± 1.6 mm	68	11.1 ± 1.5 mm

Weight-averaged molar weight of DegraPol® DP30 decreased significantly from 77.6 ± 5.7 kDa at T=0 days to 26.1 ± 6.7 kDa at T = 28 days, see **Figure 2**. Approximately half of this decrease occurred within the first 7 days (51%), whereas the decrease continued more gradually (T = 7 to 14

days: 19%, T = 14 to 21 days: 16%, T = 21 to 28 days: 14%). Biostable DegraPol® DP0 was analysed at T = 0 and 28 days only (n = 1) and did not exhibit a change in M_W.

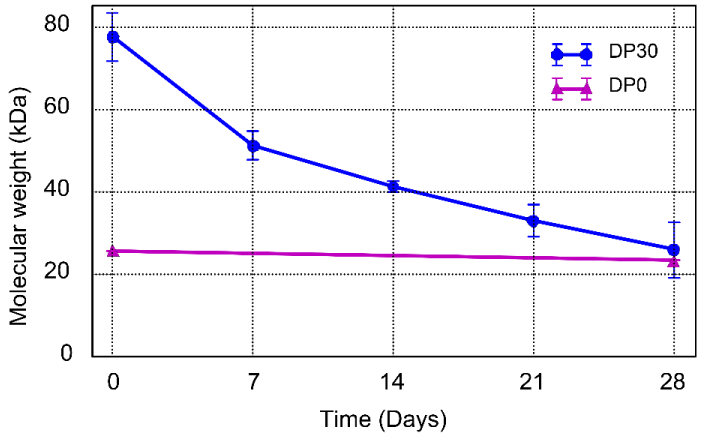

Figure 2. Molecular weight of DegraPol® DP0 and DP30 samples submerged in PBS versus exposure time up to 28 days.

Tissue ingrowth after 28 days was slightly higher, although not statistically significant, in DegraPol® DP0 scaffolds (83 ± 10%) compared to DegraPol® DP30 scaffolds (77 ± 4%). The progress of tissue ingrowth throughout the study is illustrated in representative micrographs of H&E sections of the scaffolds and quantified in **Figure 3**.

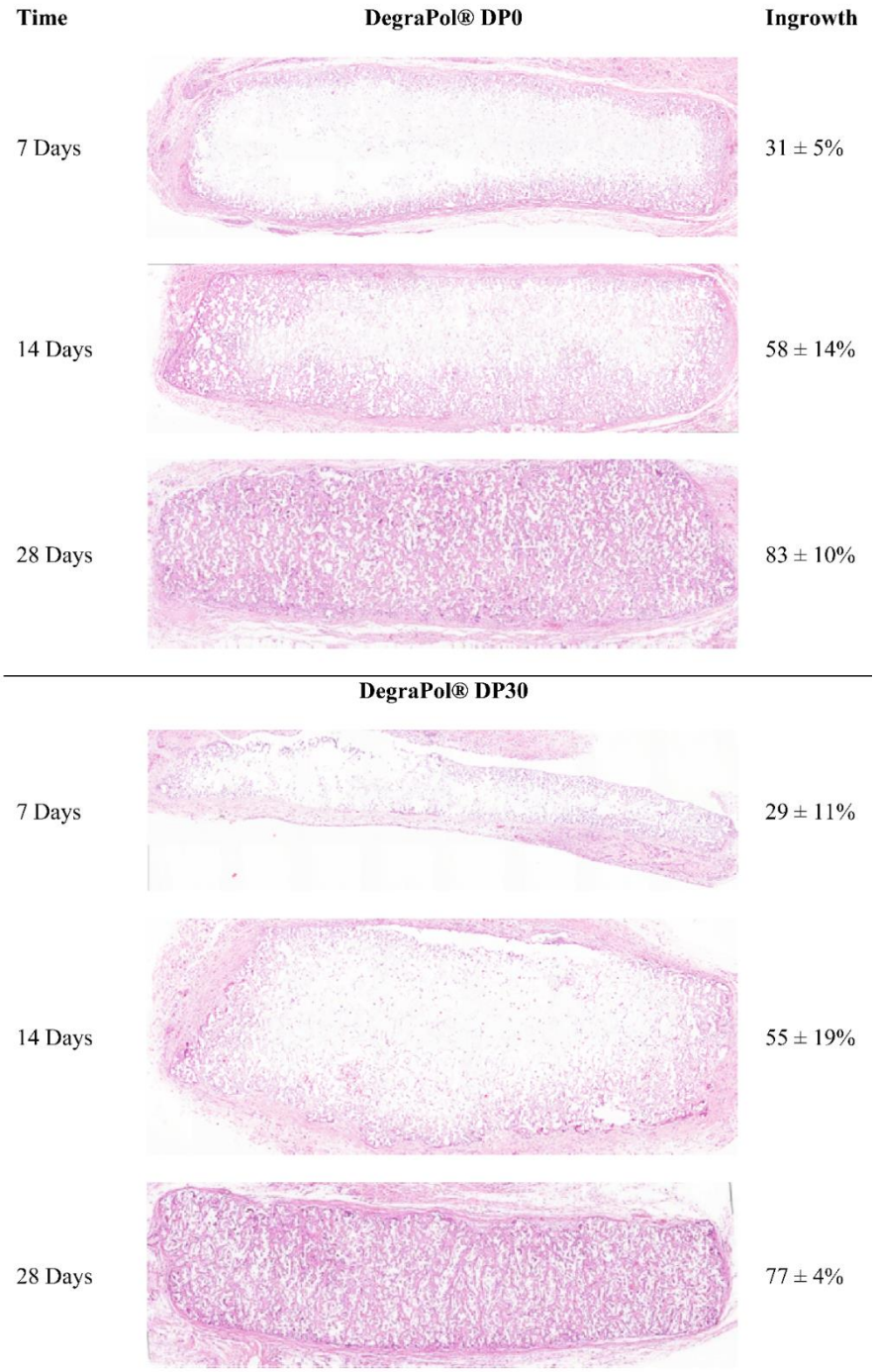

Figure 3. Histology micrographs of H&E sections in mid region of DegraPol® DP0 and DP30 scaffold samples and extent of tissue ingrowth after 7, 14 and 28 days of implantation.

Figure 4 (a) shows stress-strain data for axial and circumferential directions of pre-implant scaffold samples with and without load cycling. The resulting axial and circumferential stress scaling functions $S_C(\varepsilon)$ are illustrated in **Figure 4** (b). These functions quantify the impact of the load cycling for strains up to 16%. Disregarding data for strain below 2% (due to low signal-to-noise ratio), it was observed

for axial DegraPol® DP0 scaffold samples that load cycling reduced the stress, σ_{Cycled}, to 0.43% of the stress of non-cycled scaffolds, $\sigma_{Noncycled}$, for strain, ε, between 2% and 12%. For $\varepsilon \geq 12\%$, load cycling decreased the stress to $\sigma_{Cycled} = 0.33\ \sigma_{Noncycled}$, indicating further weakening of the scaffold. For circumferential DegraPol® DP0 samples, σ_{Cycled} gradually increased from 0.20 $\sigma_{Noncycled}$ at $\varepsilon = 2\%$ to 0.59 $\sigma_{Noncycled}$ at $\varepsilon = 12\%$ strain, and decreased to 047 $\sigma_{Noncycled}$ at $\varepsilon = 16\%$. For DegraPol® DP30 scaffold, load cycling resulted in stress between $\sigma_{Cycled} = 0.80\ \sigma_{Noncycled}$ at $\varepsilon = 2\%$ and σ_{Cycled}, = 0.98 $\sigma_{Noncycled}$ at $\varepsilon = 12\%$ and 16% in axial scaffold direction, compared to $\sigma_{Cycled} = 0.26\ \sigma_{Noncycled}$ at $\varepsilon = 2\%$, 0.93 $\sigma_{Noncycled}$ at $\varepsilon = 12\%$, and 0.97 $\sigma_{Noncycled}$ at $\varepsilon = 16\%$ in circumferential scaffold direction.

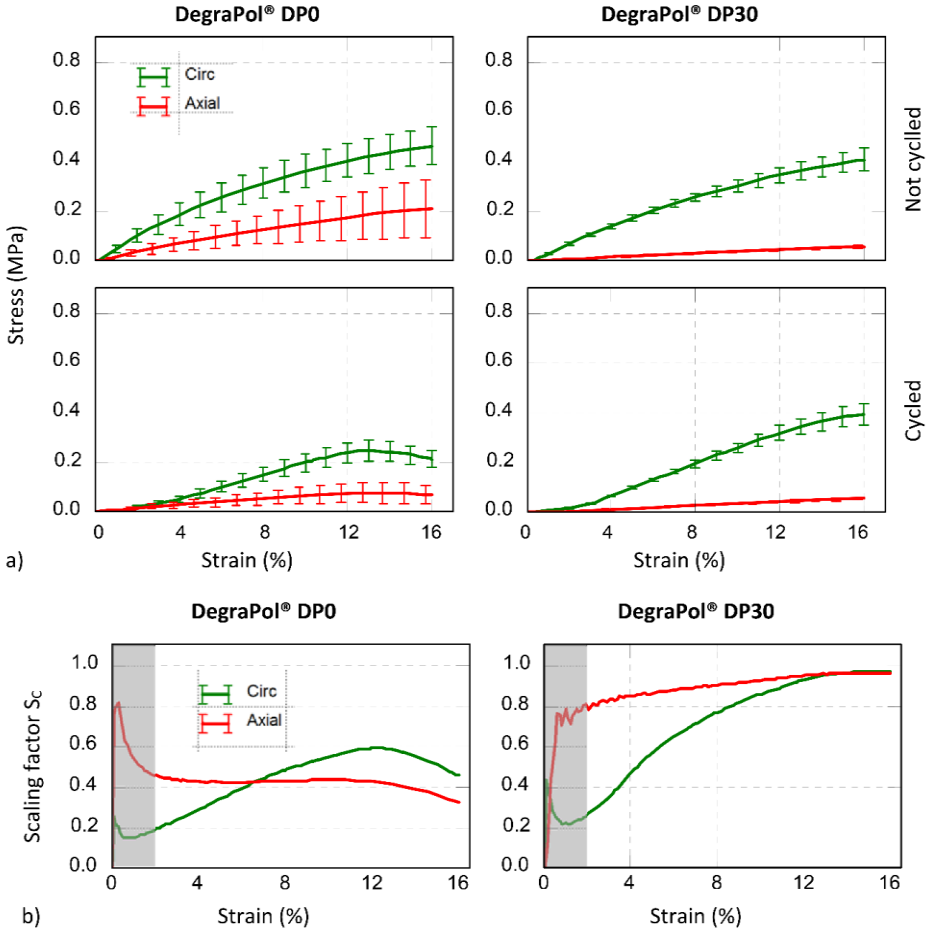

Figure 4. a) Stress versus strain curves for circumferential and axial direction of DegraPol ® DP0 and DP30 scaffolds before implantation (T = 0 day) for tensile loading protocol without and with load cycling; b) Stress scaling factor $S_C = \sigma_{Cycled}/\sigma_{Noncycled}$ versus strain, obtained from data shown in (a), representing the effect of load cycling on stress-strain behaviour of DegraPol ® DP0 and DP30. Data for strains below 2% were not considered due to high signal-to-noise ratio of force data based on low force magnitudes.

Figure 5 illustrates stress-strain data obtained without load cycling as measured for DegraPol® DP0 and DP30 scaffolds in circumferential and axial directions at the various time points of the study. Stress-strain data after incorporation of the effect of load cycling using the stress scaling function $S_C(\varepsilon)$ are provided in **Figure 6**; the mechanical characteristics $\sigma_{12\%}$, $\sigma_{16\%}$, $E_{6\%}$ and $E_{12\%}$ are shown in **Figure 7**. The changes of stress and elastic modulus from 0 to 14 and from 14 to 28 days are summarized in **Table 2**.

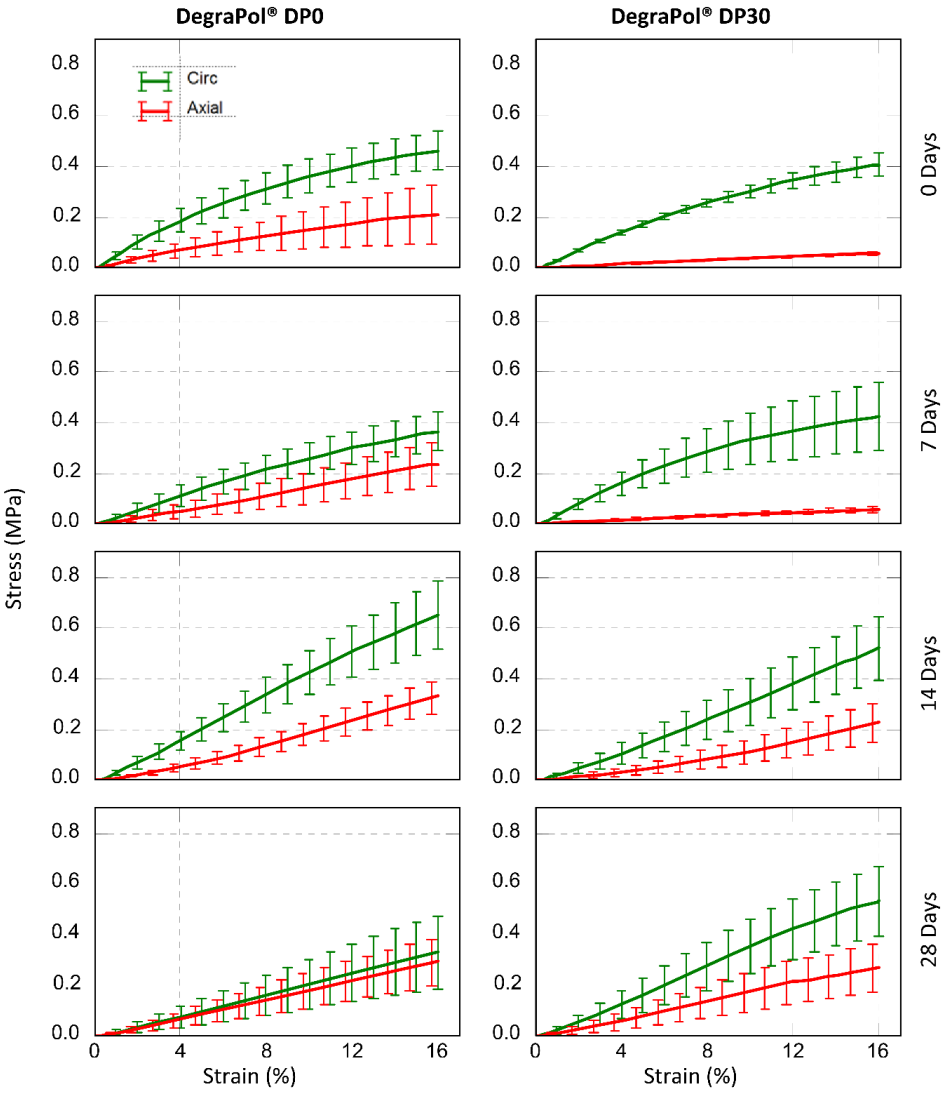

Figure 5. Stress versus strain curves for circumferential and axial direction of DegraPol ® DP0 and DP30 scaffolds without load cycling before implantation (0 day) and after implantation for T = 7, 14 and 28 days.

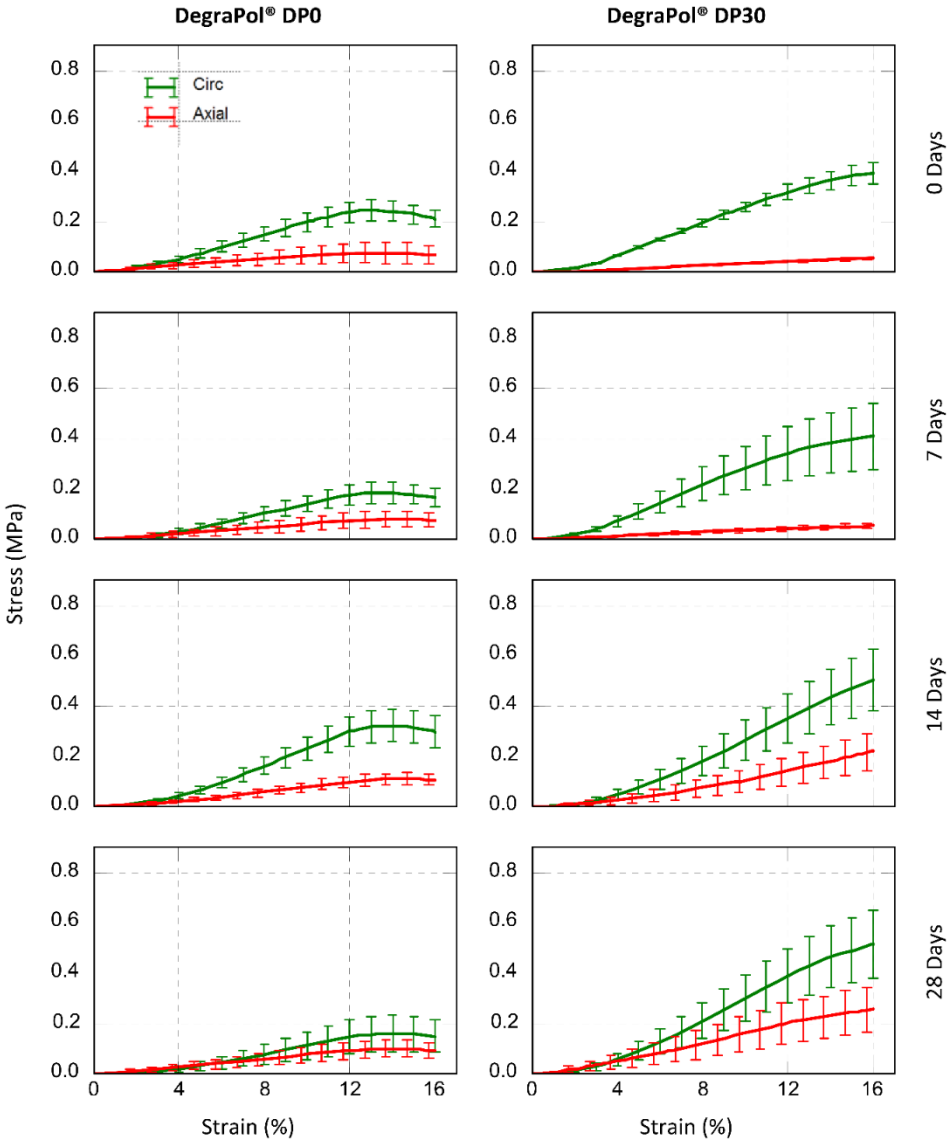

Figure 6. Stress adjusted for load cycling versus strain curves for circumferential and axial direction of DegraPol ® DP0 and DP30 scaffolds before implantation (0 day) and after implantation for T = 7, 14 and 28 days.

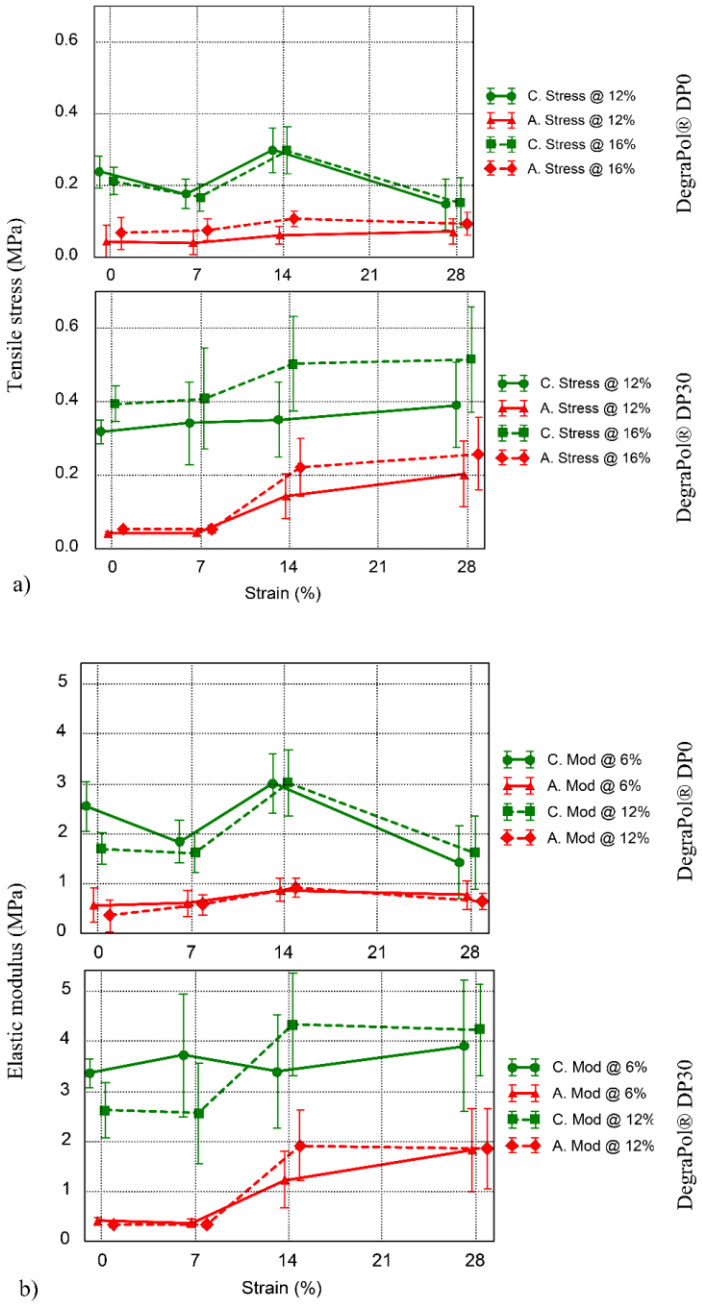

Figure 7. a) Stress at a strain of 12% and 16% versus implantation time and (b) elastic modulus at a strain of 6% and 12% versus implantation time for the circumferential (C) and axial (A) direction of DegraPol® DP0 and DP30 scaffold implants.

Table 2. Changes in stress and elastic modulus characteristics from 7 to 14 and 14 to 28 days for DegraPol® DP0 ($p < 0.05$ for all values).

Parameter	Change from T = 7 to 14 days	Change from T = 14 to 28 days
$\sigma_{12\%}$	+67%	-57%
$\sigma_{16\%}$	+78%	-49%
$E_{6\%}$	+63%	-52%
$E_{12\%}$	+87%	-46%

4. Discussion

The current study facilitated the paired *in vivo* assessment of the mechanics of biostable and degradable electrospun scaffolds based on the same polyester-urethane formulation to isolate the effects of material degradation and tissue formation after implantation. Biostable and biodegradable polyester-urethane scaffolds were implanted in the same animal.

The mechanical properties of biostable DegraPol® DP0 and degradable DegraPol® DP30 were found to be in the same range, although different responses were observed over implantation time. For DegraPol® DP0, circumferential data, but not axial, showed a significant increase from T = 7 to 14 days, and a significant decrease from T = 14 to 28 days in all characteristic measures, namely stress at 12% and 16% strain, and elastic modulus at 6% and 12% strain (**Table 2**). DegraPol® DP30 scaffolds exhibited a significant increase in stiffness *in vivo*. Whereas $E_{6\%}$ did not change, $E_{12\%}$ increased between T = 7 to 14 days by 50% ($p < 0.05$) for circumferential samples and by 213% for axial samples. This increase in elastic modulus was not reflected in the stress of circumferential samples but was for axial samples. Stress at 16% remained constant between T= 0 and 7 days but increased by 296% at T = 14 days ($p < 0.05$) and remained at that level at T = 28 days. The increase in elastic modulus after T = 7 days was linked to tissue ingrowth. Although there was approximately 30% ingrowth by 7 days, it was not yet fully interconnected throughout the scaffold, and thus did not contribute much to the overall mechanics. As tissue continued to populate the scaffold, regions with neo-tissue interconnected and developed greater structural strength.

Consistent mechanical performance from implantation through healing and scaffold degradation is highly desired for tissue-regenerative scaffolds, e.g. when used for vascular grafts. In the early phase after implantation, the circumferential stiffness in the scaffolds is based predominantly on fibres. As scaffold fibres degrade, the scaffold stiffness will decrease, unless the tissue balances out the difference. The consistency observed in circumferential stiffness of DegraPol® DP30 scaffold was thus of specific importance. Our previous *in vitro* study showed that the loss in material strength of DegraPol® DP30 predominantly occurred in the first 14 days [31], which correlated with decrease in molecular weight by T = 14 days. Assuming a similar trend for the scaffold *in vivo*, it holds that the

tissue incorporation was contributing to the overall stiffness and balancing out the loss due to degradation. The stability in circumferential mechanical response contrasts, however, with the results by Teutelink et al. [36] where the grafts not implanted were significantly stiffer than the neo-vessels explanted after 90 days.

DegraPol® DP0 and DP30 scaffolds both featured a substantial degree of fibre alignment. However, DegraPol® DP0 scaffolds showed higher fibre alignment than DegraPol® DP30 scaffolds ($p < 0.05$), with high goodness values for the Gaussian fits of the fibre dispersion data in both cases (**Table 1**).

Tissue ingrowth was similar in DegraPol® DP0 and DP30 scaffolds, although it appeared to be slightly slower in the latter (**Figure 3**). Levels of tissue ingrowth increased significantly between all subsequent time points of the study for both DegraPol® DP0 and DP30 scaffolds ($p < 0.05$) except the increase between T = 14 and 28 days for DegraPol® DP30.

In order to avoid inducing premature damage in DegraPol® scaffold samples at later time points of the study, load cycling was not included in the protocol for mechanical characterisation. However, the effect of load cycling was characterised for pre-implant scaffolds and applied to scaffolds retrieved at the various time points. DegraPol® DP0 scaffolds displayed a higher sensitivity to load cycling than the DP30 scaffolds. For DP0 scaffolds, the stress scaling parameter S_C ranging between 0.20 and 0.59 indicates that load cycling reduced stress in the scaffold by at least 41%. In addition, the decrease in stress $\sigma_{Noncycled}$ (**Figure 4**(a) bottom left panel) and stress scaling parameter S_C (**Figure 4**(b) left panel) for strain above 12% indicates damage induced in the DegraPol® DP0 scaffold due to load cycling) both in direction of and transverse to the fibre alignment. For DegraPol® DP30, S_C ranged between 0.26 and 0.98 across the strain range studied. The DegraPol® DP0 scaffolds showed a more substantial weakening due to pre-cycling when compared to the DegraPol® DP30 scaffolds.

DegraPol® DP0 scaffolds were significantly more aligned than DegraPol® DP30, with a mean dispersion angle of less than 10°, compared to >17° for DegraPol® DP30. DegraPol® DP30 scaffolds also showed more fibre merging than DegraPol® DP0, another possible factor. Lee et al. [37] reported similar behaviour in Pellethane® electrospun meshes. They indicated that a higher degree of fibre merging resulted in better distribution of load compared to an otherwise similar structure with lesser fibre merging. Low degrees of fibre merging led to a structure in which the load was not as readily distributed among fibres, resulting in earlier onset of failure of individual fibres, and consequently the entire mesh. This correlated with the observation that DegraPol® DP30 fibres displayed more merging and higher tolerance to cyclic loading than the DegraPol® DP0 scaffolds. In addition, higher alignment led to individual fibres experiencing higher strains at low scaffold strain and thus failing earlier, as the fibres were already straight and thus did not need to first straightened out [38]. Again, the scaffold morphology correlated with tensile test results, with the higher aligned DegraPol® DP0

scaffolds incurring more damage at lower strains, as reflected by the decrease in stress post 12% strain.

5. Conclusions

Considering our previous *in vitro* observation that the DegraPol® DP30 scaffold loses its material strength predominantly during the first 14 days of hydrolytic degradation, the consistency of the elastic modulus of the degradable scaffold between 14 and 28 days in the current study is an indication that the regenerated tissue construct retains its mechanical properties. The strain stiffening of the tissue constructs with DegraPol® DP30 scaffold from 7 days of implantation onwards (evidenced through the increase of elastic modulus from 6% to 12% strain) is an additional advantage and mechanical behaviour observed in soft biological tissues such as blood vessels. For the application of the scaffold as tissue regenerative vascular grafts, further research is required to indicate whether similar results will be obtained in the circulatory implant position.

References

1. Williams DF (2006) To engineer is to create: the link between engineering and regeneration. Trends Biotechnol 24 (1):4-8. doi:DOI: 10.1016/j.tibtech.2005.10.006

2. Furth ME, Atala A, Van Dyke ME (2007) Smart biomaterials design for tissue engineering and regenerative medicine. Biomaterials 28 (34):5068-5073

3. Ratcliffe A (2000) Tissue engineering of vascular grafts. Matrix Biology 19 (4):353-357

4. Chlupac J, Filova E, Bacakova L (2009) Blood vessel replacement: 50 years of development and tissue engineering paradigms in vascular surgery. Physiological Research 58 Suppl 2:S119-139. doi:931918 [pii]

5. Berglund JD, Galis ZS (2003) Designer blood vessels and therapeutic revascularization. British Journal of Pharmacology 140 (4):627-636. doi:10.1038/sj.bjp.0705457

6. Wang X, Lin P, Yao Q, Chen C (2007) Development of Small-Diameter Vascular Grafts. World Journal of Surgery 31 (4):682-689. doi:10.1007/s00268-006-0731-z

7. Teo W-E, Ramakrishna S (2009) Electrospun nanofibers as a platform for multifunctional, hierarchically organized nanocomposite. Composites Science and Technology 69 (11–12):1804-1817. doi:http://dx.doi.org/10.1016/j.compscitech.2009.04.015

8. Zilla P, Bezuidenhout D, Human P (2007) Prosthetic vascular grafts: Wrong models, wrong questions and no healing. Biomaterials 28 (34):5009-5027

9. Limbert G, Omar R, Krynauw H, Bezuidenhout D, Franz T (2016) The anisotropic mechanical behaviour of electro-spun biodegradable polymer scaffolds: Experimental characterisation and constitutive formulation. J Mech Behav Biomed Mater 53:21-39. doi:http://dx.doi.org/10.1016/j.jmbbm.2015.07.014

10. Ritter EF, Fata MM, Rudner AM, Klitzman B (1998) Heparin bonding increases patency of long microvascular prostheses. Plastic and Reconstructive Surgery 101 (1):142-146

11. Gosselin C, Vorp DA, Warty V, Severyn DA, Dick EK, Borovetz HS, Greisler HP (1996) ePTFE Coating with Fibrin Glue, FGF-1, and Heparin: Effect on Retention of Seeded Endothelial Cells. Journal of Surgical Research 60 (2):327-332. doi:DOI: 10.1006/jsre.1996.0052

12. Herring M, Smith J, Dalsing M, Glover J, Compton R, Etchberger K, Zollinger T (1994) Endothelial seeding of polytetrafluoroethylene femoral popliteal bypasses: the failure of low-density seeding to improve patency. Journal of Vascular Surgery 20 (4):650-655. doi:0741-5214(94)90291-7 [pii]

13. Mooney DJ, Baldwin DF, Suh NP, Vacanti JP, Langer R (1996) Novel approach to fabricate porous sponges of poly(-lactic-co-glycolic acid) without the use of organic solvents. Biomaterials 17 (14):1417-1422

14. Pennel T, Zilla P, Bezuidenhout D (2013) Differentiating transmural from transanastomotic prosthetic graft endothelialization through an isolation loop-graft model. Journal of Vascular Surgery 58 (4):1053-1061

15. Murphy WL, Dennis RG, Kileny JL, Mooney DJ (2002) Salt Fusion: An Approach to Improve Pore Interconnectivity within Tissue Engineering Scaffolds. Tissue Engineering 8 (1):43-52. doi:doi:10.1089/107632702753503045

16. Jun H-W, West JL (2005) Endothelialization of Microporous YIGSR/PEG-Modified Polyurethaneurea. Tissue Engineering 11 (7-8):1133-1140. doi:doi:10.1089/ten.2005.11.1133

17. Nam YS, Park TG (1999) Biodegradable polymeric microcellular foams by modified thermally induced phase separation method. Biomaterials 20 (19):1783-1790. doi:Doi: 10.1016/s0142-9612(99)00073-3

18. Nam YS, Park TG (1999) Porous biodegradable polymeric scaffolds prepared by thermally induced phase separation. Journal of Biomedical Materials Research 47 (1):8-17. doi:10.1002/(sici)1097-4636(199910)47:1<8::aid-jbm2>3.0.co;2-l

19. Bergmeister H, Schreiber C, Grasl C, Walter I, Plasenzotti R, Stoiber M, Bernhard D, Schima H (2013) Healing characteristics of electrospun polyurethane grafts with various porosities. Acta Biomater 9 (4):6032-6040. doi:http://dx.doi.org/10.1016/j.actbio.2012.12.009

20. Hasan A, Memic A, Annabi N, Hossain M, Paul A, Dokmeci MR, Dehghani F, Khademhosseini A (2014) Electrospun scaffolds for tissue engineering of vascular grafts. Acta Biomater 10 (1):11-25. doi:http://dx.doi.org/10.1016/j.actbio.2013.08.022

21. Hu J-J, Chao W-C, Lee P-Y, Huang C-H (2012) Construction and characterization of an electrospun tubular scaffold for small-diameter tissue-engineered vascular grafts: A scaffold membrane approach. J Mech Behav Biomed Mater 13:140-155. doi:10.1016/j.jmbbm.2012.04.013

22. McClure MJ, Sell SA, Simpson DG, Walpoth BH, Bowlin GL (2010) A three-layered electrospun matrix to mimic native arterial architecture using polycaprolactone, elastin, and collagen: A preliminary study. Acta Biomater 6 (7):2422-2433. doi:DOI: 10.1016/j.actbio.2009.12.029

23. Hong JK, Madihally SV (2011) Next Generation of Electrosprayed Fibers for Tissue Regeneration. Tissue Engineering Part B-Reviews 17 (2):125-142. doi:10.1089/ten.teb.2010.0552

24. Vatankhah E, Semnani D, Prabhakaran MP, Tadayon M, Razavi S, Ramakrishna S (2014) Artificial neural network for modeling the elastic modulus of electrospun polycaprolactone/gelatin scaffolds. Acta Biomater 10 (2):709-721. doi:http://dx.doi.org/10.1016/j.actbio.2013.09.015

25. Wu H, Fan J, Chu C-C, Wu J (2010) Electrospinning of small diameter 3-D nanofibrous tubular scaffolds with controllable nanofiber orientations for vascular grafts. J Mater Sci Mater Med 21 (12):3207-3215. doi:10.1007/s10856-010-4164-8

26. Ayres CE, Bowlin GL, Pizinger R, Taylor LT, Keen CA, Simpson DG (2007) Incremental changes in anisotropy induce incremental changes in the material properties of electrospun scaffolds. Acta Biomater 3 (5):651-661

27. de Valence S, Tille JC, Giliberto JP, Mrowczynski W, Gurny R, Walpoth BH, Möller M (2012) Advantages of bilayered vascular grafts for surgical applicability and tissue regeneration. Acta Biomater 8 (11):3914-3920. doi:http://dx.doi.org/10.1016/j.actbio.2012.06.035

28. Zhu M, Wang K, Mei J, Li C, Zhang J, Zheng W, An D, Xiao N, Zhao Q, Kong D, Wang L (2014) Fabrication of highly interconnected porous silk fibroin scaffolds for potential use as vascular grafts. Acta Biomater 10 (5):2014-2023. doi:http://dx.doi.org/10.1016/j.actbio.2014.01.022

29. Henry JJD, Yu J, Wang AJ, Lee R, Fang J, Li S (2017) Engineering the mechanical and biological properties of nanofibrous vascular grafts for in situ vascular tissue engineering. Biofabrication 9 (3). doi:10.1088/1758-5090/aa834b

30. Jirofti N, Mohebbi-Kalhori D, Samimi A, Hadjizadeh A, Kazemzadeh GH (2018) Small-diameter vascular graft using co-electrospun composite PCL/PU nanofibers. Biomedical Materials 13 (5):055014. doi:10.1088/1748-605x/aad4b5

31. Krynauw H, Bruchmüller L, Bezuidenhout D, Zilla P, Franz T (2011) Degradation-induced changes of mechanical properties of an electro-spun polyester-urethane scaffold for soft tissue regeneration. J Biomed Mater Res, Part B 99B (2):359-368. doi:10.1002/jbm.b.31907

32. Krynauw H, Buescher J, Koehne J, Verrijt L, Limbert G, Davies NH, Bezuidenhout D, Franz T (2019) Tissue ingrowth markedly reduces mechanical anisotropy and stiffness in fibre direction of highly aligned electrospun polyurethane scaffolds. bioRxiv:779942

33. Milleret V, Simonet M, Bittermann AG, Neuenschwander P, Hall H (2009) Cyto- and hemocompatibility of a biodegradable 3D-scaffold material designed for medical applications. J Biomed Mater Res B Appl Biomater 91 (1):109-121. doi:10.1002/jbm.b.31379

34. Schindelin J, Arganda-Carreras I, Frise E, Kaynig V, Longair M, Pietzsch T, Preibisch S, Rueden C, Saalfeld S, Schmid B, Tinevez J-Y, White DJ, Hartenstein V, Eliceiri K, Tomancak P, Cardona A (2012) Fiji: an open-source platform for biological-image analysis. Nat Meth 9 (7):676-682

35. Woolley AJ, Desai HA, Steckbeck MA, Patel NK, Otto KJ (2011) In situ characterization of the brain–microdevice interface using Device Capture Histology. J Neurosci Methods 201 (1):67-77. doi:http://dx.doi.org/10.1016/j.jneumeth.2011.07.012

36. Teutelink A, van der Laan MJ, Milner R, Blankensteijn JD (2003) Fabric tears as a new cause of type III endoleak with Ancure endograft. J Vasc Surg 38 (4):843-846

37. Lee K, Lee B, Kim C, Kim H, Kim K, Nah C (2005) Stress-strain behavior of the electrospun thermoplastic polyurethane elastomer fiber mats. Macromol Res 13 (5):441-445. doi:10.1007/bf03218478

38. Mauck RL, Baker BM, Nerurkar NL, Burdick JA, Li WJ, Tuan RS, Elliott DM (2009) Engineering on the straight and narrow: the mechanics of nanofibrous assemblies for fiber-reinforced tissue regeneration. Tissue Eng Part B Rev 15 (2):171-193. doi:10.1089/ten.TEB.2008.0652